Available online at www.sciencedirect.com
ScienceDirect
Journal of Power Sources 174 (2007) 1201–1205
JOURNAL OF POWER SOURCES
www.elsevier.com/locate/jpowsour

Short communication

Macroporous $Li(Ni_{1/3}Co_{1/3}Mn_{1/3})O_2$: A high-rate positive electrode for rechargeable lithium batteries

K.M. Shaju, Peter G. Bruce *

EaStChem, School of Chemistry, University of St. Andrews, St. Andrews KY16 9ST, UK

Available online 26 June 2007

Abstract

Macroporous $Li(Ni_{1/3}Co_{1/3}Mn_{1/3})O_2$ synthesized by a simple non-hydroxide route has been characterize as a high-energy and high-power positive electrode for rechargeable lithium batteries, exhibiting a discharge capacity of 195 mAh g^{-1} at 1 C (2244 Wh L^{-1}) and 175 mAh g^{-1} at 10 C (2008 Wh L^{-1}) and 99.99% capacity retention. Note the volumetric calculations are based on composite electrodes, not just the volume of the active material. Comparison between macroporous $Li(Ni_{1/3}Co_{1/3}Mn_{1/3})O_2$ and the material synthesized by the conventional hydroxide method demonstrates that the latter shows a significant increase in polarization upon cycling whereas the former material does not. Cycling at 50 °C shows that the macroporous material does exhibit more polarization at elevated temperatures. Macroporous $Li(Ni_{1/3}Co_{1/3}Mn_{1/3})O_2$ has been tested with a graphite negative electrode in a rocking-chair cell. Cycling was inferior to that with a Li metal negative electrode, but the origin of this may lie with the negative electrode. Powder X-ray diffraction also collected on macroporous $Li(Ni_{1/3}Co_{1/3}Mn_{1/3})O_2$ after 100 cycles to 4.2 and 4.6 V, shows excellent structural stability, whereas cycling to 4.2 V induces a reduction in the Li/Ni site exchange from 4% to 2%, no significant change occurs for cycling to 4.6 V.

Keywords: Lithium-ion battery; $Li(Ni_{1/3}Co_{1/3}Mn_{1/3})O_2$; Macroporous; Positive electrode material

1. Introduction

$Li(Ni_{1/3}Co_{1/3}Mn_{1/3})O_2$ adopts the layered $LiCoO_2$ structure (α-$NaFeO_2$ structure type) in which Ni, Co and Mn occupy the octahedral sites in the transition metal layers and Li occupies the octahedral sites in the alkali metal layers [1–10]. The lower cost and superior safety compared with $LiCoO_2$ has resulted in $Li(Ni_{1/3}Co_{1/3}Mn_{1/3})O_2$ replacing $LiCoO_2$ in advanced rechargeable lithium-ion batteries, where the new electrode delivers comparable energy density over a similar voltage range [1,4,5,11–17]. However, there is much current interest in materials that can deliver higher energy density and higher power than $LiCoO_2$ for new markets. In this regard, increasing the upper voltage cut-off for $Li(Ni_{1/3}Co_{1/3}Mn_{1/3})O_2$ to 4.6 V results in delivery of a capacity approximating 200 mAh g^{-1}.

Although an attractive positive electrode material in many respects, the usual synthesis of $Li(Ni_{1/3}Co_{1/3}Mn_{1/3})O_2$ is somewhat complex, involving first the preparation of a mixed hydroxide $[(Ni_{1/3}Co_{1/3}Mn_{1/3})OH_2]$ or carbonate $[(Ni_{1/3}Co_{1/3}Mn_{1/3})CO_3]$, then reaction with a lithium source to form the final product [1,2,5–8,18]. Recently, we reported a simpler, one-step, synthesis of $Li(Ni_{1/3}Co_{1/3}Mn_{1/3})O_2$ that involves mixing all the precursors together in solution along with resorcinol and formaldehyde, then heating in a controlled manner to form the desired phase with a disordered macroporous morphology [19]. The resulting material is not only straightforward to synthesis but also delivers superior performance to $Li(Ni_{1/3}Co_{1/3}Mn_{1/3})O_2$ prepared by the hydroxide-based route [19]. A capacity of 195 mAh g^{-1} is obtained at a rate of 1 C, with a capacity retention of 99.99%, and 175 mAh g^{-1} is delivered at 10 C. These capacities correspond to practical volumetric energy densities (calculated based on the method described previously [19,20]) of 2244 Wh L^{-1} (1 C) and 2008 Wh L^{-1} (10 C) (based on the volume of the composite electrode, not just the active material), indicating that the macroporous material delivers high-rate performance (power) without compromising significantly the volumetric energy density [19]. In summary, macroporous $Li(Ni_{1/3}Co_{1/3}Mn_{1/3})O_2$ can deliver high-power and high-energy density.

Results, demonstrating the successful one-step synthesis of macroporous $Li(Ni_{1/3}Co_{1/3}Mn_{1/3})O_2$, its structure, composition and basic electrochemical performance were presented in our

* Corresponding author.
E-mail address: P.G.Bruce@st-andrews.ac.uk (P.G. Bruce).

0378-7753/$ – see front matter © 2007 Elsevier B.V. All rights reserved.
doi:10.1016/j.jpowsour.2007.06.091

previous paper [19]. Here we present further characterization of the performance, including load curves as a function of rate, comparison between $Li(Ni_{1/3}Co_{1/3}Mn_{1/3})O_2$ synthesized by the one-step process and material prepared by the mixed hydroxide route, and the first results from a rocking-chair cell composed of a graphite negative electrode and a macroporous $Li(Ni_{1/3}Co_{1/3}Mn_{1/3})O_2$ positive electrode.

2. Experimental

Synthesis of macroporous $Li(Ni_{1/3}Co_{1/3}Mn_{1/3})O_2$ was carried out as reported previously [19]. In brief, $LiCH_3COO{\cdot}2H_2O$, $Ni(CH_3COO)_2{\cdot}4H_2O$, $Co(CH_3COO)_2{\cdot}4H_2O$ and $Mn(CH_3COO)_2{\cdot}4H_2O$ (Fluka; ≥99%) were dissolved in quantities corresponding to 0.02 mol of stoichiometric $Li(Ni_{1/3}Co_{1/3}Mn_{1/3})O_2$ in 60 ml of water, containing 0.1 mol of resorcinol (Fluka; 99%), 0.15 mol of formaldehyde (Fluka; 36.5% in water, methanol-stabilized) and 0.5 m mol of Li_2CO_3. The resulting solution contained a 5 mol% excess of Li. The mixture was heated at 60 °C until viscous, then 90 °C for 24 h, followed by calcination at 950 °C for 24 h to obtain macroporous $Li(Ni_{1/3}Co_{1/3}Mn_{1/3})O_2$. All procedures were carried out in air. Synthesis of $Li(Ni_{1/3}Co_{1/3}Mn_{1/3})O_2$ by the mixed hydroxide method is described in detail elsewhere [5]. The precursor, $(Ni_{1/3}Co_{1/3}Mn_{1/3})(OH)_2$ was mixed with a stoichiometric amount (1.05 Li in the starting composition) of $LiOH{\cdot}H_2O$, the mixture was ground and the powder pressed into pellets. The pellets were initially heated to 480 °C for 4 h. The product was cooled, reground, pellets were formed and heated at 950 °C for 24 h, followed by cooling to room temperature.

Powder X-ray diffraction (PXRD) was carried out using a Stoe STADI/P diffractometer operating in transmission mode using a Fe source to minimise fluracence from manganese in the sample. X-rays were collected with a small-angle position sensitive detector. Rietveld refinement was carried out using FullProf [21]. A JEOL JSM-5600 scanning electron microscope (SEM) was used for morphological studies.

To evaluate electrochemical performance, composite positive electrodes were constructed by mixing the active material, Kynar 2801 (a copolymer based on PVDF) and super S carbon, in the weight ratios 76:12:12. The mixture was prepared as a slurry in *N*-methyl-pyrrolidinone (NMP) and spread onto aluminium foil using the doctor blade technique. Following evaporation of the solvent and drying, electrodes were incorporated into an electrochemical cell (coin cell NRC 2325) in which the counter electrode was formed from lithium metal and the electrolyte was LP 30 (Merck; 1 M $LiPF_6$ in 1:1 (v/v) EC:DMC). For the rocking-chair cells, a composite negative electrode was constructed in a similar manner to the composite positive electrode, with graphite (SLP 30, Timcal), super S carbon and Kynar in the weight ratios 85:5:10. Electrochemical measurements were carried out using a Maccor Series 4200 battery cycler. In order to study the structure and morphology of the positive electrode material after cycling, the cells were dismantled in the glove box washed three times with DMC and vacuum dried. For the PXRD measurements, the electrode was sealed between Mylar films.

3. Results and discussion

Previous PXRD, ICP and SEM studies indicated that the material obtained by the one-step synthesis was layered stoichiometric $Li(Ni_{1/3}Co_{1/3}Mn_{1/3})O_2$ (i.e. no excess Li) with 4% exchange of Li and Ni between the layers and with a macroporous morphology, Fig. 1 [19]. The macroporous morphology, composed of 0.5–1 μm particles fused together to form the macropores, is retained on electrode fabrication and on cycling. The variation of discharge capacity with discharge rate was also presented in our previous paper [19]. Here we provide more detailed information concerning the variation of voltage with state-of-charge, at different rates, Fig. 2. An upper cut-off potential of 4.6 V was used in each case, since we wish to explore the performance of the material as a high-capacity (approximately 200 mAh g^{-1}) positive electrode. As can be seen in Fig. 2 the discharge profile is smooth and relatively invariant on changing the rate from 20 mA g^{-1} (*C*/10) to 4000 mA g^{-1} (20*C*).

In Fig. 3 we compare the variation of voltage with state-of-charge, on charge and discharge, for our macroporous material and $Li(Ni_{1/3}Co_{1/3}Mn_{1/3})O_2$ prepared by the conventional hydroxide route, which does not have the macroporous morphology and for which the particle size is 1–2 μm. The composite positive electrodes were constructed identically. Again charging was carried out to 4.6 V in order to explore the performance of the material when delivering a high capacity. In

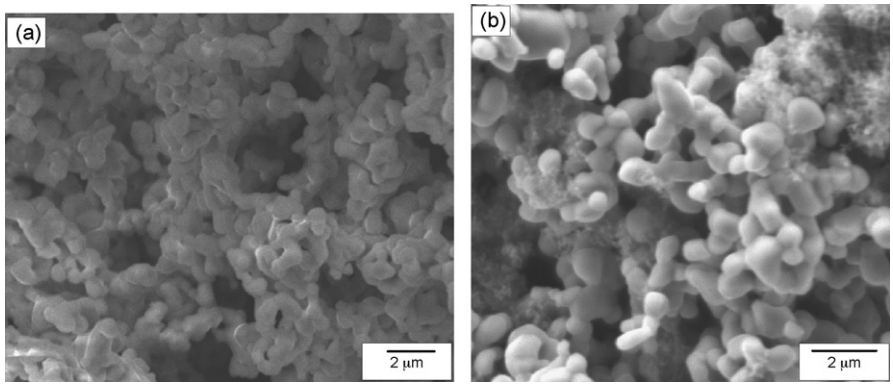

Fig. 1. SEM images of (a) as-prepared $Li(Ni_{1/3}Co_{1/3}Mn_{1/3})O_2$ and (b) an electrode after 100 cycles between 2.5 and 4.6 V at 100 mA g^{-1}.

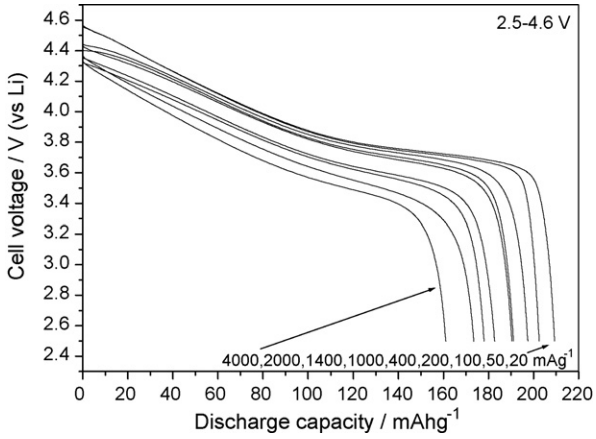

Fig. 2. The variation of voltage with state of charge, at different discharge rates (shown) for macroporous $Li(Ni_{1/3}Co_{1/3}Mn_{1/3})O_2$. The cell was charged at 100 mA g^{-1} to 4.6 V then held at this voltage such that the total charging time was 3.0 h (CCCV mode), before discharging to 2.5 V. Data were collected on the same cell.

both cases, the initial charge capacity exceeds that on the subsequent discharge by ~30 mAh g^{-1}. This irreversible capacity has been noted previously by other authors [2,5–7,10,11]. The first discharge capacity for the macroporous material at 100 mA g^{-1} (*C*/2) is 209 mAh g^{-1} compared with a value of 175 mAh g^{-1} for the material made by the hydroxide route. The charge and discharge curves for the macroporous material remain remarkably invariant on cycling. The shape changes very little and the separation between the charge and discharge curves is small, remaining invariant on cycling, capacity retention was 99.99% per cycle. This contrasts sharply with the load curves for the material obtained from the hydroxide route. Although

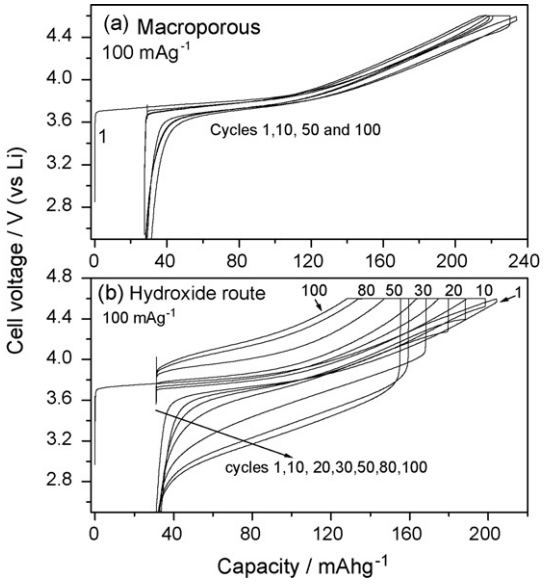

Fig. 3. Variation of voltage with state of charge for selected cycles on charge and discharge, (a) macroporous $Li(Ni_{1/3}Co_{1/3}Mn_{1/3})O_2$ and (b) $Li(Ni_{1/3}Co_{1/3}Mn_{1/3})O_2$ prepared by the conventional hydroxide route. Cycling was carried out at 100 mA g^{-1} in the voltage range 2.5–4.6 V. From the second cycle onwards the total charging time was set to 3 h (CCCV mode). Cycle numbers are shown.

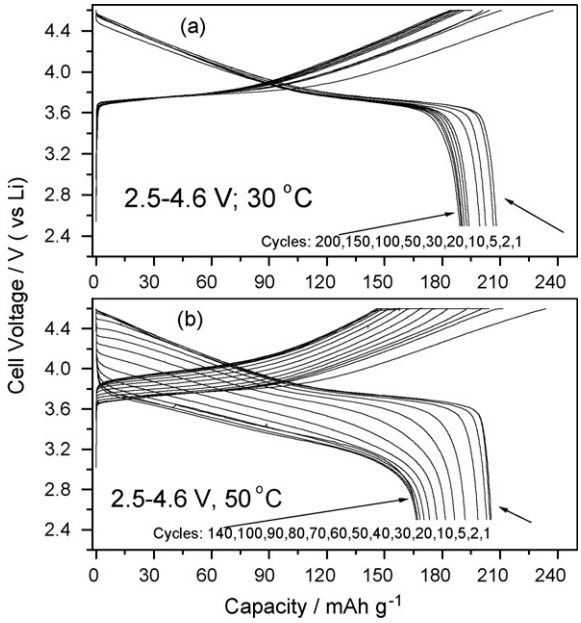

Fig. 4. Comparison of the charge and discharge voltage profiles at 100 mA g^{-1} for selected cycles of macroporous $Li(Ni_{1/3}Co_{1/3}Mn_{1/3})O_2$ charged to 4.6 V and cycled at 30 and 50 °C.

initially (1–10 cycles) the separation between charge and discharge curves is similar to that for the macroporous material, thereafter the charge and discharge curves increasingly diverge, indicating that a significant polarization develops upon cycling. The increasing polarization leads to a significant degradation in capacity on cycling for the hydroxide based material, something that is not observed for the macroporous material.

As well as operation at room temperature, the performance of the material at elevated temperatures is important. Comparison of the charge and discharge profiles for selected cycles of macroporous $Li(Ni_{1/3}Co_{1/3}Mn_{1/3})O_2$ charged to 4.6 V and cycled at 30 and 50 °C are shown in Fig. 4. The data in Fig. 4a extend those from Fig. 3a by adding more cycles. Fig. 4a also presents the data in a form that permits direct comparison with the data at 50 °C in Fig. 4b. The shapes of the load curves on charge and discharge at the two temperatures are very similar, as are the initial charge and discharge capacities. The charge/discharge capacities show an initial decrease (1–20 cycles at 30 °C and 1–50 cycles at 50 °C) and thereafter remain relatively stable on continued cycling. The polarization at 50 °C is seen to be more pronounced, resulting in more capacity fading. This could be due to instability of the electrolyte at this elevated temperature, leading to more severe SEI film formation on the active material surface, more work is underway to investigate the origin of the 50 °C fade.

The performance of macroporous $Li(Ni_{1/3}Co_{1/3}Mn_{1/3})O_2$ in a rocking-chair cell has been explored by combining it with a graphite negative electrode. The cells were constructed such that their capacities were positive electrode limited. Pre-cycled graphite electrodes were used for assembling the Li-ion cells in order to minimize the Li consumption from the positive electrode during the first charge [22]. Before cell assembly, the graphite electrode was subjected to three discharge/charge

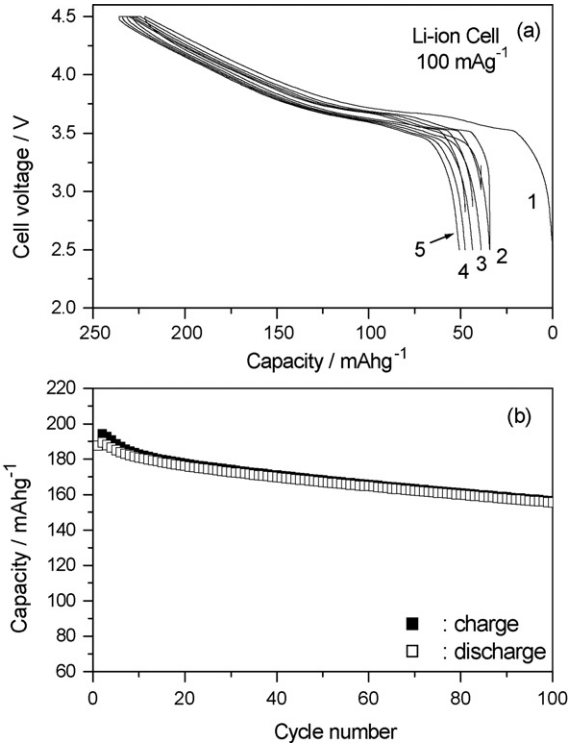

Fig. 5. (a) The variation of voltage with state of charge for the rocking-chair cell (graphite/Li($Ni_{1/3}Co_{1/3}Mn_{1/3}$)O_2) cycled between 2.5 and 4.5 V at 100 mA g^{-1} and (b) variation of charge and discharge capacities on cycling the above cell.

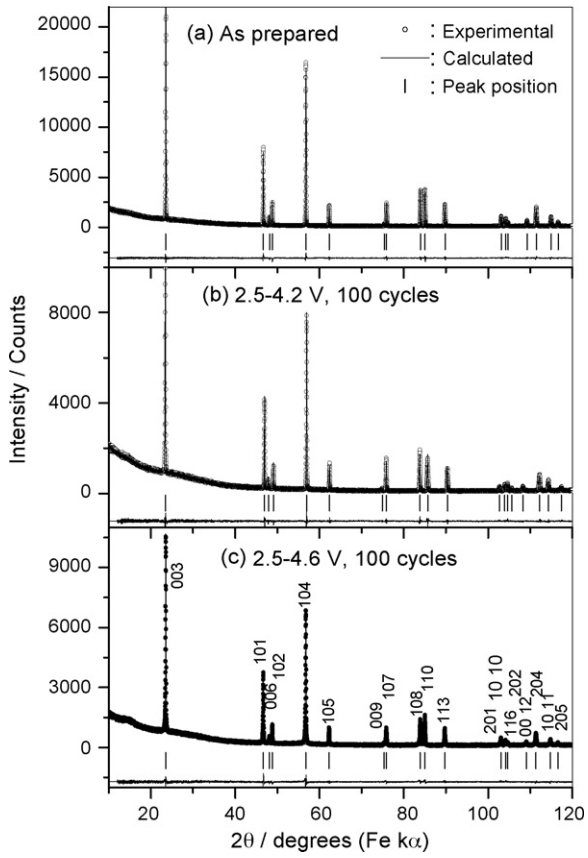

Fig. 6. Powder X-ray diffraction patterns (Rietveld refinement) for Li($Ni_{1/3}Co_{1/3}Mn_{1/3}$)O_2 as-synthesized, at the end of discharge after 100 cycles when cycled to 4.2 and 4.6 V cut-offs.

cycles using Li metal as the counter electrode, in the voltage range, 0.005–3.00 V at 50 mA g^{-1}. The variation of voltage with state-of-charge on cycling between 2.5 and 4.5 V for the rocking chair cell is shown in Fig. 5a for the first five cycles. Since pre-cycled graphite was used, the irreversible capacity loss on the first cycle is the same as that observed in Fig. 3b. The voltage profiles are smooth and relatively invariant on cycling. The capacity fade of the Li-ion cell is shown in Fig. 4b. The initial discharge capacity is 188 mAh g^{-1}, dropping to 182 mAh g^{-1} after 10 cycles, thereafter the rate of fade decreases on cycling, with a capacity of 157 mAh g^{-1} being obtained after 100 cycles (average capacity fade rate is 0.16% per cycle). This capacity fading is significant compared with the same positive electrode cycled against a lithium metal electrode at the same rate and over the same voltage range (0.01% per cycle on cycling to 4.6 V versus Li). A cell cycled with the same graphite against a Li metal electrode exhibited similar capacity fade. Therefore, we expect the fade is related to the negative electrode.

Previously, studies have been carried out on the variation of structure with lithium content on the first extraction and then reinsertion of lithium in $Li_x(Ni_{1/3}Co_{1/3}Mn_{1/3})O_2$ [8,10,11,13]. Structural integrity on repeated cycling has also been reported, but no detailed analysis given [14]. PXRD obtained for macroporous Li($Ni_{1/3}Co_{1/3}Mn_{1/3}$)O_2 at the end of discharge after 100 cycles is shown in Fig. 6. Cycling was carried out between 2.5 and 4.2 V, i.e. an upper voltage cut-off comparable to that used in commercial cells. The PXRD data indicate that there is no major structural degradation on repeated cycling. Structure refinement using the Rietveld method shows a decrease in Li/Ni disorder from 4.0% (as prepared) to 2% (after 100 cycles). The refined unit cell parameters were: as prepared: $a = 2.8647(1)$ Å and $c = 14.2464(1)$ Å; after 100 cycles: $a = 2.8430(1)$ Å and $c = 14.3330(1)$ Å. Thus a slight expansion in the c axis and contraction in the a parameter occurs on cycling. The lattice parameters of the cycled electrode are close to that reported for the partially delithiated phase, $Li_{0.84}(Ni_{1/3}Co_{1/3}Mn_{1/3})O_2$ with 2.3% Li/Ni exchange [10]. By counting the charge passed during charge and discharge (taking into account the irreversible capacity loss on the first cycle) it is possible to estimate the amount of Li at the end of discharge after 100 cycles, $Li_{0.842}(Ni_{1/3}Co_{1/3}Mn_{1/3})O_2$. This is in reasonable agreement with the composition reported by Nazar and co-workers with similar lattice parameters [10]. Also from the charge passed, it is possible to estimate the composition range over which cycling takes place, $0.28 < x < 0.84$. It has been shown that on chemical extraction of Li from $Li_x(Ni_{1/3}Co_{1/3}Mn_{1/3})O_2$ the O3 structure begins to convert to O1 below $x = 0.30$ [10]. The excellent cycling stability in the voltage range, 2.5–4.2 V has previously been ascribed to such cycling being carried within the O3 structure. However, cycling stability is also excellent for our macroporous material over the voltage range 2.5–4.6 V, which, the charge passed, corresponds to the composition range, $0.04 < x < 0.73$ after 100 cycles. Such a composition range is expected to intrude into the O1 phase and involve the O1–O3

transformation on each cycle. PXRD at the end of discharge for macroporous $Li(Ni_{1/3}Co_{1/3}Mn_{1/3})O_2$ after 100 cycles between 2.5 and 4.6 V confirms the high degree of structural stability for this material, Fig. 6c. Rietveld refinement indicated that cycling to 4.6 V does not alter the Li/Ni site exchange significantly, which remains at 4% and the cell parameters were: $a = 2.8661(1)$ Å and $c = 14.2618(1)$ Å. Refinement was carried out on the composition, $Li_{0.73}(Ni_{1/3}Co_{1/3}Mn_{1/3})O_2$, based on the charge passed.

4. Conclusions

Macroporous $Li(Ni_{1/3}Co_{1/3}Mn_{1/3})O_2$ has been compared with the same material synthesized by the hydroxide route and the latter shown to suffer a significant increase in polarization on cycling compared with the former. Comparison of the voltage profiles for macroporous material at 30 and 50 °C showed that, although the voltage curves were smooth at higher temperatures, polarization does increase. The first results from a rocking-chair cell composed of a graphite negative electrode and macroporous $Li(Ni_{1/3}Co_{1/3}Mn_{1/3})O_2$ were presented and indicated that capacity fading is greater for the rocking-chair cell compared with cycling against a Li metal negative electrode. PXRD data after extended cycling of the macroporous $Li(Ni_{1/3}Co_{1/3}Mn_{1/3})O_2$ to 4.2 and 4.6 V indicate excellent structural integrity in accord with the high degree of capacity retention. Whereas cycling to 4.2 V does decrease the Li/Ni site exchange from 4% to 2%, no significant change occurs on cycling to 4.6 V.

Acknowledgements

PGB is indebted to the EPSRC (SUPERGEN) and The Royal Society for financial support.

References

[1] T. Ohzuku, Y. Makimura, Chem. Lett. (2001) 642.
[2] N. Yabuuchi, Y. Koyama, N. Nakayama, T. Ohzuku, J. Electrochem. Soc. 152 (2005) A1434.
[3] Z. Lu, D.D. MacNeil, J.R. Dahn, Electrochem. Solid State Lett. 4 (2001) A200.
[4] D.D. MacNeil, Z. Lu, J.R. Dahn, J. Electrochem. Soc. 149 (2002) A1332.
[5] K.M. Shaju, G.V. Subba Rao, B.V.R. Chowdari, Electrochim. Acta 48 (2002) 145.
[6] T.-H. Cho, S.-M. Park, M. Yoshio, Chem. Lett. 33 (2004) 704.
[7] S.H. Park, H.-S. Shin, S.-T. Myung, C.S. Yoon, K. Amine, Y.-K. Sun, Chem. Mater. 17 (2005) 6.
[8] J. Choi, A. Manthiram, J. Electrochem. Soc. 152 (2005) A1714.
[9] M.-H. Lee, Y.-J. Kang, S.-T. Myung, Y.-K. Sun, Electrichim. Acta 50 (2004) 939.
[10] S.-C. Yin, Y.-H. Rho, I. Swainson, L.F. Nazar, Chem. Mater. 18 (2006) 1901.
[11] N. Yabuuchi, T. Ohzuku, J. Power Sources 119–121 (2003) 171.
[12] T. Nukuda, T. Inamasu, A. Fujii, D. Endo, H. Nakagawa, S. Kozono, T. Iguchi, J. Kuratomi, K. Kohno, S. Izuchi, M. Oshitani, J. Power Sources 146 (2005) 611.
[13] G.-H. Kim, J.-H. Kim, S.-T. Myung, C.S. Yoon, Y.-K. Sun, J. Electrochem. Soc. 152 (2005) A1707.
[14] I. Belharouak, Y.-K. Sun, J. Liu, K. Amine, J. Power Sources 123 (2003) 247.
[15] K.M. Shaju, G.V. Subba Rao, B.V.R. Chowdari, J. Electrochem.Soc. 151 (2004) A1324.
[16] B.J. Hwang, Y.W. Tsai, D. Carlier, G. Ceder, Chem. Mater. 15 (2003) 3676.
[17] S.-T. Myung, M.-H. Lee, S. Komaba, N. Kumagai, Y.-K. Sun, Electrochim. Acta 50 (2005) 4800.
[18] T.H. Cho, S.M. Park, M. Yoshio, T. Hirai, Y. Hideshima, J. Power Sources 142 (2005) 306.
[19] K.M. Shaju, P.G. Bruce, Adv. Mater. 18 (2006) 2330.
[20] S. Jouanneau, K.W. Eberman, L.J. Krause, J.R. Dahn, J. Electrochem. Soc. 150 (2003) A1637.
[21] Fullprof, available at URL, http://www-llb.cea.fr/winplotr/winplotr.htm.
[22] I.R.M. Kottaegoda, Y. Kodoma, H. Ikuta, Y. Uchimoto, M. Wakihara, J. Electrochem. Soc. 152 (2005) A1595.